

Strong Electron-Phonon Interaction and Colossal Magnetoresistance in EuTiO_3

Ruofan Chen, Ji-Chang Ren, Km Rubi, R. Mahendiran, and Jian-Sheng Wang

Department of Physics, National University of Singapore, Singapore 117551, Republic of Singapore

(Dated: September 20, 2017)

At low temperatures, EuTiO_3 system has very large resistivities and exhibits colossal magnetoresistance. Based on a first principle calculation and the dynamical mean-field theory for small polaron we have calculated the transport properties of EuTiO_3 . It is found that due to electron-phonon interaction the conduction band may form a tiny polaronic subband which is close to the Fermi level. The tiny subband is responsible for the large resistivity. Besides, EuTiO_3 is a weak antiferromagnetic material and its magnetization would slightly shift the subband via exchange interaction between conduction electrons and magnetic atoms. Since the subband is close to the Fermi level, a slight shift of its position gives colossal magnetoresistance.

I. INTRODUCTION

The colossal magnetoresistance (CMR) observed in manganites (doped $\text{R}_{1-x}\text{A}_x\text{MnO}_3$ oxides, where R and A are trivalent rare earth and divalent alkaline ions respectively) has attracted much attention for the past two decades¹⁻⁵, not only for its possible utility in technology but also for a better theoretical understanding of magnetoresistance. Reports on magnetoresistance in rare earth titanates of formula RTiO_3 are scarce because of their large resistivities at low temperature. Recently our experiments find that the undoped perovskite titanium oxide EuTiO_3 exhibits CMR below 40K: with the presence of an external magnetic field its resistivity drops dramatically. In our experiments, polycrystalline EuTiO_3 sample was prepared using standard solid state reaction method in reduced atmosphere (95% Ar and 5% H_2). More details about the sample preparation can be found in Refs^{6,7}. The DC resistivity was measured in a Physical Property Measurement System (Quantum Design Inc, USA) using an electrometer in two probe configuration. Experimental resistivities are shown in Fig. 1. Due to the low temperature and the large resistivity, whether CMR in EuTiO_3 is useful in practice is not clear yet, but an investigation on it may broaden our theoretical understanding of CMR.

When the external magnetic field is absent, the resistivity ρ of EuTiO_3 decreases exponentially with increasing temperature like in a semiconductor:

$$\rho \approx \rho_0 e^{\Delta E/k_B T}, \quad (1)$$

where ΔE is the gap between the bottom of conduction band and the Fermi level, and ρ_0 is large and weakly temperature dependent. The curve of ρ can be fitted by an exponential function $e^{152.53/x+6.66}$, and substituting this fitting into Eq. (1) we obtain that $\Delta E \approx 152.53 k_B K \approx 0.013 \text{ eV}$, which is a small value. With such a small gap, a relatively high carrier density is expected. However, this contradicts with large resistivities shown in the figure, which are mostly larger than $10^5 \Omega \cdot \text{cm}$. This paradox indicates that, rather than applying the theory of semiconductor directly, some other factors need to be considered.

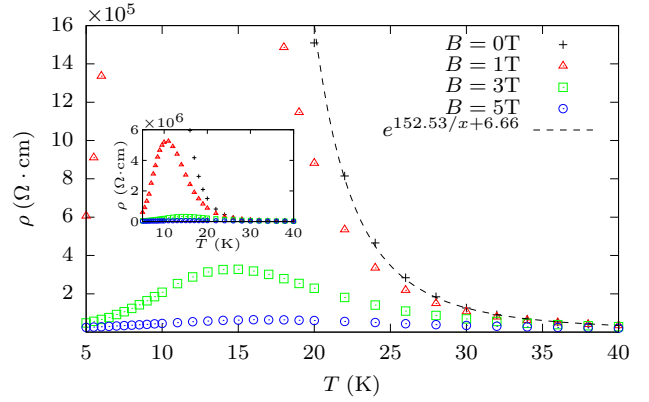


FIG. 1. (color online) Experimental resistivities of EuTiO_3 . A function $y = e^{152.53/x+6.66}$ is used to fit the experimental resistivity without magnetic field, where $y = \rho/(\Omega \cdot \text{cm})$ and $x = T/\text{K}$. The inset represents the same data but with a larger scale.

II. THE MODEL

It has been reported in literature¹⁻⁵ that electron-phonon, especially polaronic, interaction plays an important role in CMR. Millis¹ pointed out that in the $\text{La}_{1-x}\text{Sr}_x\text{MnO}_3$ double exchange alone can not explain its resistivity, and Jahn-Teller effect must be considered. Later Zhao⁵ showed that in $\text{La}_{1-x}\text{Sr}_x\text{MnO}_3$ the electron transport behaviour is consistent with small polaron coherent motion which involves a strong coupling between electrons and soft optical phonons. And the small polaron effect had also been observed in a titanium oxide, rutile (TiO_2), single crystal⁸. Therefore we also take strong electron-phonon interaction into consideration and use small polaron formalism to model it in EuTiO_3 at low temperature.

The ions $\text{Eu}^{2+}(4f^7)$ in EuTiO_3 have a large localized spin ($S = 7/2$), which is the source of magnetism. The magnetic properties of EuTiO_3 can be described by an antiferromagnetic Heisenberg model⁹ and Weiss mean-field theory, and the Néel temperature of the crystal is about 5.4 K ^{7,10,11}. The magnetization \mathbf{M} is defined to be a dimensionless quantity as $2\langle \hat{S} \rangle$ and M is the abso-

lute magnitude $|\mathbf{M}|$, here a Landé factor 2 is included. The mean-field calculation of M as a function of temperature T and magnetic field B is shown as the inset of Fig. 2. The conduction electrons (t_{2g} orbitals electrons of Ti) are assumed to be coupled with magnetic atoms (Eu) via simple exchange interaction¹², and such interaction would cause shift of the conduction band when the system is magnetized. As will be shown later, such shift is responsible for CMR. Note that unlike the case in the double exchange model, the conduction electron and the magnetic atom are not at the same site, i.e., the exchange interaction is not intraatomic. Therefore the strength of exchange interaction is supposed to be small and the scattering by magnetic atoms may be neglected. The smallness of exchange interaction also implies that the material has a fine electronic structure if the CMR effect is due to this interaction.

It can be also seen from the insert of Fig. 2 that in the presence of magnetic field the magnetization increases, while the resistivity drops dramatically, with decreasing temperature and increasing magnetic field. This reminds us that the drop of resistivities may be related to the increase of magnetization.

In this article the electron-phonon interaction is assumed to be the Holstein model type¹³⁻¹⁵, which means that conduction electrons are coupled with local dispersionless optical phonons. The Hamiltonian is written in two parts as

$$\hat{H} = \hat{H}_0 + \hat{H}_1, \quad (2)$$

where

$$\begin{aligned} \hat{H}_0 = & - \sum_{ij,\alpha} t_{ij} \hat{c}_{i\alpha}^\dagger \hat{c}_{j\alpha} + \omega_0 \sum_i \hat{a}_i^\dagger \hat{a}_i \\ & + g \sum_{i\alpha} \hat{c}_{i\alpha}^\dagger \hat{c}_{i\alpha} (\hat{a}_i + \hat{a}_i^\dagger) \end{aligned} \quad (3)$$

is the Holstein model Hamiltonian. Here t_{ij} is the hopping matrix element connecting site i and j , and the operator $\hat{c}_{i\alpha}^\dagger$ ($\hat{c}_{i\alpha}$) creates (destroys) an electron with spin α at site i while \hat{a}_i^\dagger (\hat{a}_i) creates (destroys) a phonon at site i . The frequency of the optical phonon is denoted by ω_0 and the coupling strength of electron-phonon interaction is denoted by g . The coupling between electrons and magnetic atoms is expressed by the exchange interaction

$$\hat{H}_1 = J \sum_i \hat{\mathbf{s}}_i \cdot \mathbf{M}(T, B), \quad (4)$$

where J is the corresponding coupling strength, the operator $\hat{\mathbf{s}}_i$ is electron spin operator $\sum_{\alpha\beta} \hat{c}_{i\alpha}^\dagger \frac{1}{2} \boldsymbol{\sigma}_{\alpha\beta} \hat{c}_{i\beta}$ at site i with $\boldsymbol{\sigma}_{\alpha\beta}$ the Pauli matrices vector and \mathbf{M} is the magnetization of the material which is a function of temperature and magnetic field.

Back to Eq. (1), it should be emphasized that although the thermal activated hopping process of small polaron gives the same form of resistivity^{15,16}, Eq. (1) is unlikely due to this process. This can be argued as follows. There

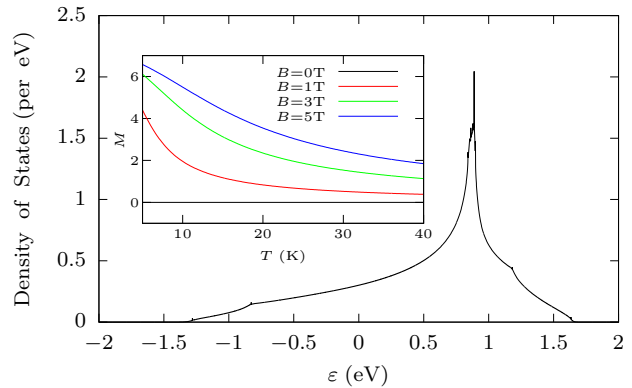


FIG. 2. (color online) The DOS by first principle calculation. The Fermi level, which need to be fitted by experimental data later, is not specified here. The first principle DFT calculation is carried out within the spin-polarized generalized gradient approximation (GGA)²² using norm-conserving pseudopotentials. We use a kinetic energy cutoff of 60 Ry and a $10 \times 10 \times 10$ Γ -centered k -point mesh for the unit cell simulations. Then the mesh is interpolated up to $40 \times 40 \times 40$ by Wannier functions. The inset represents the mean-field calculation of magnetization of EuTiO_3 , here $M = |\mathbf{M}|$ is defined as a dimensionless quantity.

exists a crossover temperature where the polaron motion crosses over from band like to thermal activated hopping motion, and the hopping process begins to dominate when temperature is above such crossover temperature. This crossover temperature should be around $0.4\omega_0$ ¹⁴⁻¹⁶. According to the first principle calculation the highest frequency of optical phonon is about 0.1 eV¹⁷, and we assume it to be the value of ω_0 . This value means that the crossover temperature should be around 464 K, which is far above 40 K. Besides, experiments showed that the crossover temperature of rutile (TiO_2) is about 300 K⁸, which is also far above 40 K.

III. THE METHOD

To obtain the electronic structure of a specified material which involves strong interaction, the method combining first principle calculation and dynamical mean-field theory (DMFT) are often used^{18,19}. In this article the density of states (DOS) of conduction band (t_{2g} orbitals of Ti atom) is obtained via first principle calculation. Then based on this DOS we apply the DMFT for the small polaron^{14,15}, which is a method for Holstein model, to handle electron-phonon interaction. According to the DMFT results, due to electron-phonon coupling it is possible to form a tiny polaronic subband of the conduction band near the Fermi level. Such a tiny subband would reduce both the carrier density and electrical mobility. The existence of such a tiny subband may be the explanation of the coexistence of small ΔE , low carrier density and high resistivity.

The carrier density is assumed to be very small and the temperature under consideration is low, therefore we can use the zero temperature formalism of DMFT for small polaron which works in the extreme dilute limit¹⁴ to deal with \hat{H}_0 . In this formalism an analytic impurity solver can be built by continued-fraction expansion²⁰. The crucial advantage of such an impurity solver is that it allows the DMFT procedure to be done directly in real frequency domain and thus no analytic continuation is needed. The unperturbed DOS before the DMFT procedure is calculated via density functional theory (DFT) by Quantum Espresso²¹ and then interpolated by Wannier functions^{23,24}. The DOS of t_{2g} orbitals of Ti atom thus calculated is shown in Fig. 2. After the DMFT calculation for \hat{H}_0 , an energy dependent self-energy $\Sigma_0(\varepsilon)$ and the corresponding retarded Green's function $G_0(\varepsilon)$ are obtained. As mentioned earlier, the frequency of the optical phonon ω_0 is about 0.1 eV. The spectral density calculated by DMFT with \hat{H}_0 for different values of g is shown in Fig. 3, where the spectral density is given by $-\frac{1}{\pi}\text{Im}G_0(\varepsilon)$.

It can be seen from Fig. 3(a) that when g increases to 0.6 eV a small peak appears at the bottom of the band. As g goes to 0.8 eV a second peak appears and the first one becomes lower, see Fig. 3(b). It can be also seen from (c)–(e) that when g becomes larger, the first peak remains but its position is shifted. And in (f) the first peak is shifted outside the figure.

The first two peaks can be treated as two tiny subbands of the conduction band, and they can provide conduction electrons. At first glance, the first subband is too small and may be neglected. However, our calculation of resistivities shows that the second subband still provides too many conduction electrons for such large resistivities. Thus we focus on the first subband which is the polaronic subband. If this subband is close to the Fermi level, then it can explain the smallness of ΔE . And since the subband is tiny, the carrier density would be still low.

Now let us turn to \hat{H}_1 . The magnetization \mathbf{M} in \hat{H}_1 is an average quantity, which means that scatterings due to localized spins are neglected. It is easy to see that \hat{H}_1 would not change the shape of electronic band structure, but only shift the self-energy according to different spins of electrons. Therefore the final results for self-energy is $\Sigma_\alpha = \Sigma_0 \pm \frac{1}{2}JM(T, B)$ with $M = |\mathbf{M}|$ for spin up and down respectively. This is a kind of band shift. The final Green's function G_α would change according to the band shift for different spin α . And the final spectral density is then given by $-\frac{1}{\pi}\text{Im}G_\alpha$.

The static conductivity, which is the inverse of resistivity, can be calculated via the Kubo-Greenwood^{25–27} formula (here the trace contains spin summation)

$$\sigma = \frac{e^2\hbar}{\pi V} \int \left(-\frac{\partial f}{\partial \varepsilon} \right) \text{Tr}[\hat{v}_x \text{Im}G(\varepsilon) \hat{v}_x \text{Im}G(\varepsilon)] d\varepsilon, \quad (5)$$

where V is the volume of system and \hat{v}_x is the operator for a component of velocity. Here we can use Boltzmann distribution $f = \exp[(\mu - \varepsilon)/k_B T]$ instead of the Fermi-

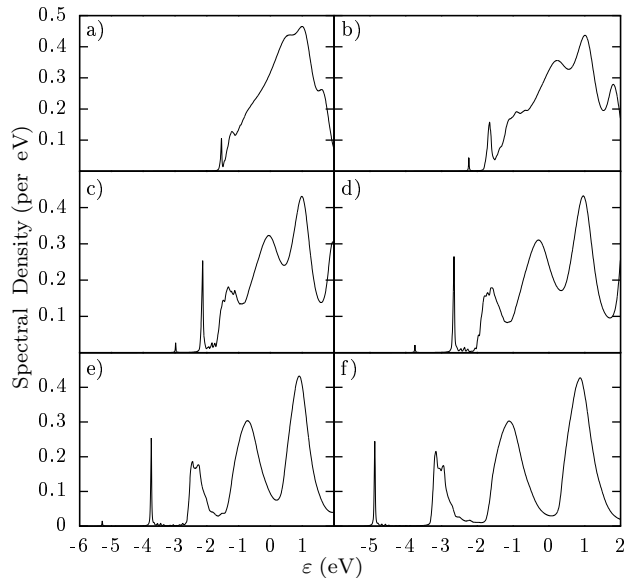


FIG. 3. The spectral density calculated by DMFT with $g =$ (a) 0.6 eV, (b) 0.8 eV, (c) 1.0 eV, (d) 1.2 eV, (e) 1.6 eV, and (f) 2.0 eV. The unperturbed DOS used by DMFT is shown in Fig. 2.

Dirac distribution since the temperature is much lower than ΔE . Due to the band shift the distribution function becomes $f = \exp[(\mu - \varepsilon \mp \frac{1}{2}JM)/k_B T]$. The band with spin down is shifted by $-\frac{1}{2}JM$, thus it goes closer to the Fermi level and provides more conduction electrons. While another band with spin up would be shifted away from the Fermi level and the carrier density in it would be reduced. However, because the distribution function is exponential, the total carrier density increases and the resistivity decreases accordingly. An important point here is that $\Delta E \approx 0.013$ eV is very small, thus even a small amount of shift, say $30 k_B K \approx 0.0026$ eV, would cause an obvious difference. While in other materials such a small amount of shift may be just ignored. This is the origin of CMR.

IV. RESULTS AND DISCUSSION

We calculate resistivities based on the first peak in Fig. 3(c) with $g = 1.0$ eV. This value of g , of course, may not be accurate for real situation, so we need to adjust our parameters to fit experimental data. More discussion about the value of g can be found in appendix. We set the Fermi level at -3.0778 eV. Note that because the carrier density is very sensitive to the band shift, the position of the Fermi level need to be carefully placed. With this Fermi level the electron occupation number per site at 20 K without magnetic field is about 8.457×10^{-7} , which is consistent with the extreme dilute limit used by DMFT. The group velocity $v_x(\mathbf{k})$ of electron is obtained by our first principle calculation. The maximum

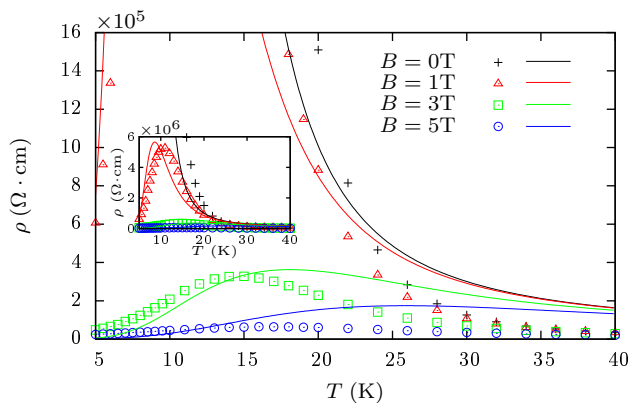


FIG. 4. (color online) Resistivities of EuTiO_3 . Solid lines represent theoretical results, and experimental data (dots) are plotted here for comparison. The inset represents the same data but with a larger scale.

velocity is about 10^5 m/s. The lattice constant of EuTiO_3 is about 4×10^{-8} cm⁹. And the value of J is set equal to 0.0025 eV $\approx 29 k_B K$. Resistivities calculated by Kubo-Greenwood formula are shown as solid lines in Fig. 4.

It can be seen that this value of J fitted by experimental data is indeed small, this confirms our assumption. And because the tiny subband is quite close to the Fermi level so such a small J still has a strong effect on the resistivity. Shapes of curves in Fig. 4 are basically controlled by the distribution function with band shift $f = \exp\{[\mu - \varepsilon \mp \frac{1}{2}JM(T, B)]/k_B T\}$. In fact, due to the band shift, the carrier density can be written in a form $n(T, B) = n_0(T)e^{\mp \frac{1}{2}JM/k_B T}$, where $n_0(T)$ is the carrier density without magnetic field. With this form of n , experimental data can be simply fitted by Einstein formula $\sigma = neb$ with a constant mobility b . The problem of this simple fitting is that either n_0 or b need to be very small. Now the existence of the tiny polaronic subband reduces both the carrier density and electrical mobility. This simple fitting is also an evidence that the band shift is the origin of CMR for EuTiO_3 .

In summary, we have applied DFT+DMFT method to calculate the electronic structure of t_{2g} orbitals of Ti atom in EuTiO_3 . Based on this electronic structure we have calculated the transport properties of EuTiO_3 and explained the CMR in it. It is found that due to polaronic interaction the conduction band can form a tiny subband. This subband may be close to the Fermi level and responsible for conduction electrons. Since the subband is very small, the carrier density is still very low even it is close to the Fermi level. This is the reason why resistivities of EuTiO_3 are quite high. Conduction electrons are also coupled with magnetic atoms via exchange interaction, and this interaction would slightly shift the electronic band when the material is magnetized. And because the subband is close to the Fermi level, a slight shift is enough to cause CMR.

It is clear that this mechanism occurs in semicon-

ductor and involves no strong intraatomic exchange interaction as in the double exchange model. Unlike in $\text{La}_{1-x}\text{Sr}_x\text{MnO}_3$ system which is metallic¹⁻⁵, the change of carrier density caused by band shift plays a main role in the CMR of EuTiO_3 . Besides, because at low temperature the carrier density for different electron spin changes dramatically when material is magnetized, EuTiO_3 has a potential for spintronic device.

Our model is a simplified model. It is not enough to obtain really the fine electronic structure of EuTiO_3 , thus the agreement with experimental data remains at a qualitative level. A more careful treatment on first principle calculation and DMFT procedure may improve the accuracy. What's more, experiments which can measure the carrier density change for different spin respectively, or just the total density change, in the presence of magnetic field can help to verify or falsify the validity of our theoretical description.

This work is supported by MOE tier 2 grant R-144-000-349-112.

Appendix A: The Value of Parameters

Here we shall discuss some details about the values of parameters ω_0 and g .

It has been mentioned earlier that the value of ω_0 is assumed to be the highest frequency optical phonon. The main reason is that the highest phonon band is well separated with other bands and is relatively flat. The flatness of the band indicates that the band is relatively local, which is consistent with the assumption of Holstein model.

The value of g is chosen to be 1 eV, it should be noted that this value is a large value for electron-phonon interaction. Especially, applying Lang-Firsov²⁸ transformation, which is the standard method for small polaron theory, on Holstein model yields some unphysical polaron parameters. The bandwidth renormalization constant for small polaron is $\exp(-g^2/\omega_0^2) = \exp(-100) = 3.72 \times 10^{-44}$, which means the bandwidth of polaron subband would be at the order of 10^{-44} and thus this subband would be so fragile that it would be immediately washed out in a real material. However, Lang-Firsov transformation also shows the position of small polaron subband should be located around $-g^2/\omega_0 = -10$ eV, which is far from the subband we obtain. Therefore what we obtain is not the fragile polaron subband but another relatively robust subband caused by strong electron-phonon interaction.

So is this large g possible? Our first principle calculation shows it is indeed possible in EuTiO_3 system.

The DFT calculations are performed using Quantum ESPRESSO package²¹. The Troullier-Martins norm-conserving pseudopotentials with the Perdew-Burke-Ernzerhof (PBE) exchange-correlation functionals²² are employed to describe the interactions between valence electrons in our system. The cutoff energies of plane

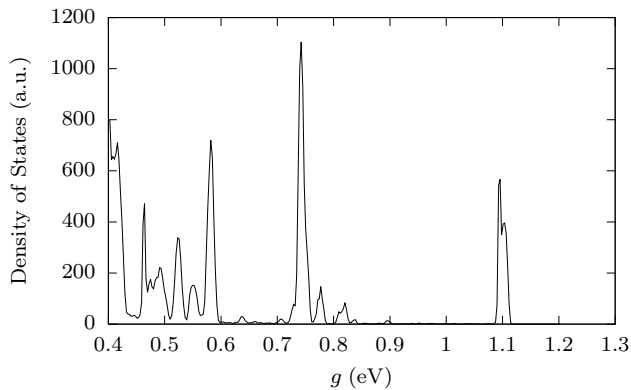


FIG. 5. Density of states of the coupling constants between electronic states with localized LO mode phonon states.

waves are chosen as 80 Ry. A $20 \times 20 \times 20$ Monkhorst-Pack k -point mesh is used for electronic self-consistent field calculations and a $4 \times 4 \times 4$ Monkhorst-Pack k -point mesh is used for phonon calculations. The convergence threshold of energy is set to be 10^{-14} Ry for electron, while for phonon calculations, the threshold is set to be 10^{-18} Ry to get a better convergence. The electron phonon coupling matrix is calculated by applying formula²⁹: $g_{m\nu}(\mathbf{k}, \mathbf{q}) = \langle u_{m\mathbf{k}+\mathbf{q}} | \Delta_{\mathbf{q}\nu} v^{\text{KS}} | u_{n\mathbf{k}} \rangle$, where $u_{n\mathbf{k}}$ is the lattice-periodic function in Bloch wavefunction, the bra and ket indicate an integral over one unit cell, and the operator $\Delta_{\mathbf{q}\nu} v^{\text{KS}}$ is the derivative with a coefficient of the self-consistent potential with respect to a collective ionic displacement corresponding to a phonon with branch index ν and momentum \mathbf{q} . In order to get a denser mesh to calculate the electron phonon coupling matrix, we apply Wannier interpolation technique, as implemented in EPW code³⁰. After Fourier transformation back into momentum space, we obtain a dense $40 \times 40 \times 40$ \mathbf{k} -point mesh for states of electron and $40 \times 40 \times 40$ \mathbf{q} -

point mesh for states of phonon.

The DFT results can be found in Fig. 5, it can be seen that the highest values of the elements of the electron-phonon coupling matrix elements are around 1.1 eV. Since Holstein model is used, in which electrons are coupled with localized phonons, we focus on the coupling between electrons and phonons of highest longitudinal optical mode. Therefore in Fig. 5 only those results of LO mode with coupling constant larger than 0.4 eV are represented. These results show that the value of g can reach about 1.1 eV, and thus our value is consistent with the DFT results.

Appendix B: The Extreme Dilute Limit

In a strongly correlated system, usually the value of electron occupation number would greatly affect the electronic spectral density. For instance, the DMFT results for $\text{La}_{1-x}\text{Sr}_x\text{MnO}_3$ system¹ differ much around half filling situation for different occupation numbers.

However, in our calculations the rigid band approximation is applied, i.e., the spectral density remains unchanged when carrier density changes. Here we shall explain the reason why we can adopt this approximation.

It has been mentioned earlier that the electron occupation number per site at 20 K without the magnetic field is about 8.457×10^{-7} , and such small occupation number enables us to apply extreme dilute limit and single electron approximation used in DMFT for small polaron. With the presence of an external magnetic field, the occupation number increases dramatically. However, even the occupation increases 1000 times, it is at an order of 10^{-4} which is still very small. Therefore we can say that during CMR the occupation number, although dramatically changes, is always small enough to apply extreme dilute limit and single electron approximation, and so the rigid band approximation. This is also an important difference between EuTiO_3 system and $\text{La}_{1-x}\text{Sr}_x\text{MnO}_3$.

¹ A. J. Millis *et al.*, Phys. Rev. Lett. **74**, 5144 (1995); Phys. Rev. Lett. **77**, 175 (1996); Phys. Rev. B. **54**, 5405 (1996); Nature, **392**, 147 (1998).
² J. Zang, A. R. Bishop and H. Röder, Phys. Rev. B. **53**, R8840 (1996); H. Röder, J. Zang and A. R. Bishop, Phys. Rev. Lett. **76**, 1356 (1996).
³ Q. Li, J. Zang, A. R. Bishop, C. M. Soukoulis, Phys. Rev. B. **56**, 4541 (1997).
⁴ R. Shen and Z.-Z. Li, Solid State Commun. **110**, 237 (1999).
⁵ G.-M. Zhao, V. Smolyaninova, W. Prellier and H. Keller, Phys. Rev. Lett. **84**, 6086 (2000).
⁶ Km Rubi and R. Mahendiran, Europhys. Lett. **118**, 57008 (2017).
⁷ A. Midya *et al.*, Phys. Rev. B. **93**, 094422 (2016).
⁸ V. N. Bogomolov *et al.*, Phys. Stat. Sol. **27**, 443 (1968); Phys. Stat. Sol. **35**, 555 (1969).

⁹ T. Katsufuji and H. Takagi, Phys. Rev. B. **64**, 054415 (2001).
¹⁰ B. P. Alho, A. M. G. Carvalho and P. J. von Ranke, J. Magn. Magn. Mater. **324**, 210 (2012).
¹¹ P. J. von Ranke *et al.*, J. Magn. Magn. Mater. **324**, 1290 (2012).
¹² C. Haas, CRC. Crit. Rev. Solid State. Sci. **1**, 47 (1970).
¹³ T. Holstein, Ann. Phys. **8**, 325 (1959); **8**, 343, (1959).
¹⁴ S. Ciuchi, F. de Pasquale, S. Fratini and D. Feinberg, Phys. Rev. B. **56**, 4494 (1997).
¹⁵ S. Fratini and S. Ciuchi, Phys. Rev. Lett. **91**, 256403 (2003).
¹⁶ G. D. Mahan, *Many-Particle Physics* (Plenum Press, New York, 2000), 3rd ed.
¹⁷ K. Z. Rushchanskii, N. A. Spaldin and M. Ležaić, Phys. Rev. B. **85**, 104109 (2012).
¹⁸ A. Georges, G. Kotliar, W. Krauth and M. J. Rozenberg,

- Rev. Mod. Phys. **68**, 13 (1996).
- ¹⁹ G. Kotliar, S. Y. Savrasov, K. Haule, V. S. Oudovenko, O. Parcollet and C. A. Marianetti, Rev. Mod. Phys. **78**, 865 (2006).
- ²⁰ V. S. Viswanath and G. Müller, *The Recursion Method* (Springer-Verlag, Berlin, 1994).
- ²¹ P. Giannozzi *et al.*, J. Phys. Condens. Matter **21**, 395502 (2009).
- ²² J. P. Perdew, K. Burke, and M. Ernzerhof, Phys. Rev. Lett. **77**, 3865 (1996).
- ²³ N. Marzari and D. Vanderbilt, Phys. Rev. B. **56**, 12847 (1997).
- ²⁴ I. Souza, N. Marzari and D. Vanderbilt, Phys. Rev. B. **65**, 035109 (2001).
- ²⁵ R. Kubo, J. Phys. Soc. Jpn. **12**, 570 (1957).
- ²⁶ D. A. Greenwood, Proc. Phys. Soc. **71**, 585 (1958).
- ²⁷ E. N. Economou, *Green's Function in Quantum Physics* (Springer-Verlag, Berlin, 2006) 3rd ed.
- ²⁸ I. G. Lang and Yu. A. Firsov, Zh. Eksp. Teor. Fiz. **43**, 1843 (1962) [Sov. Phys. JETP **16**, 1301 (1963)].
- ²⁹ F. Giustino, Rev. Mod. Phys. **89**, 015003 (2017).
- ³⁰ S. Poncé, E. R. Margine, C. Verdi and F. Giustino, Comput. Phys. Commun. **209**, 116 (2016).